iScience

CellPress
OPEN ACCESS

Article

Study of aging mechanisms in $LiFePO_4$ batteries with various SOC levels using the zero-sum pulse method

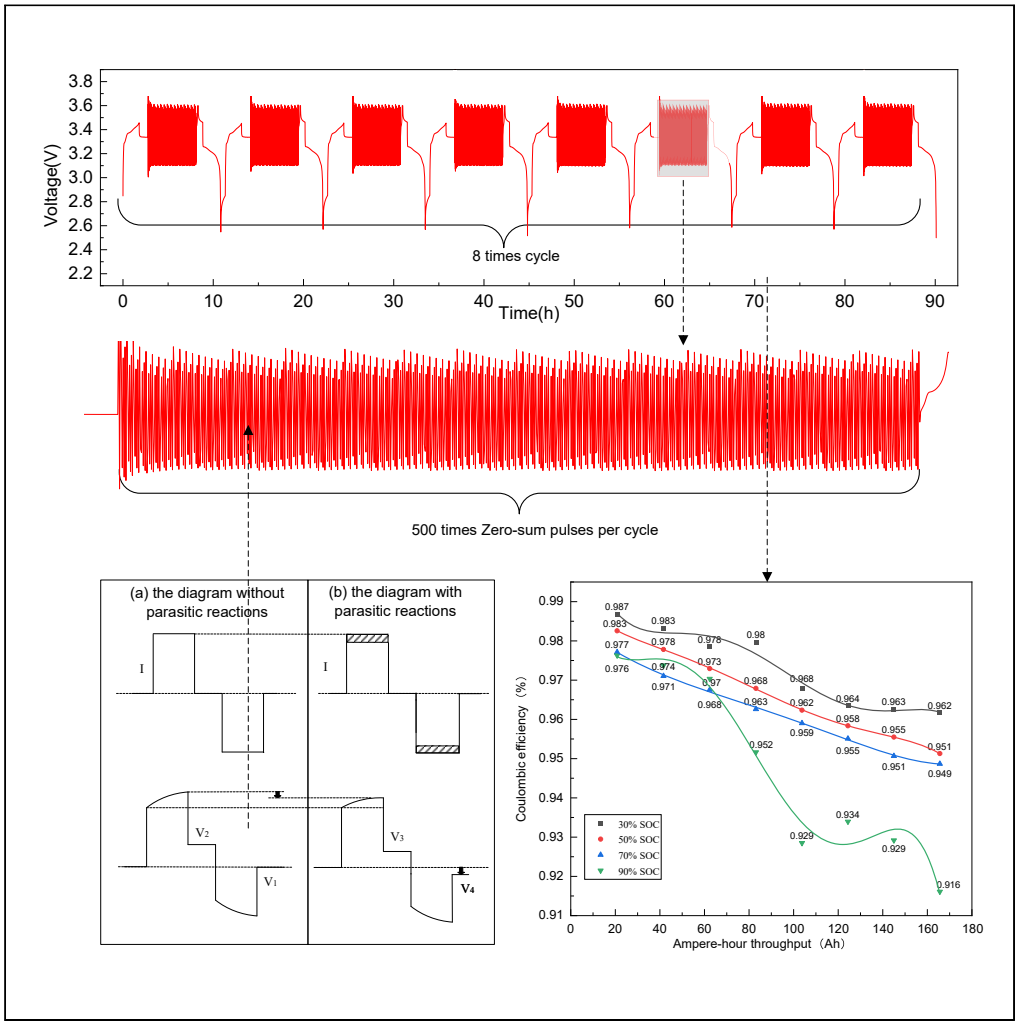

Jianqiang Kang, Guang Yang, Yongsheng Wang, Jing V. Wang, Qian Wang, Guorong Zhu

wysh@whut.edu.cn (Y.W.)
jingvwang@whut.edu.cn (J.V.W.)

Highlights

The Zero-sum pulse method is used to explore aging mechanisms under various SOC level

The Zero-sum pulse method is timeliness and accuracy

The main aging mechanism at low SOC is loss of lithium inventory

The main aging mechanism at high SOC is loss of active material

Kang et al., iScience 27, 110287
July 19, 2024
https://doi.org/10.1016/j.isci.2024.110287

iScience

CellPress
OPEN ACCESS

Article

Study of aging mechanisms in $LiFePO_4$ batteries with various SOC levels using the zero-sum pulse method

Jianqiang Kang,[1,2] Guang Yang,[1,2] Yongsheng Wang,[3,6,*] Jing V. Wang,[4,*] Qian Wang,[4] and Guorong Zhu[4,5]

SUMMARY

Investigating the correlation between aging mechanisms and state of charge (SOC) can optimize cycling conditions and prolong the life cycle of lithium-ion batteries (LIBs). A long-term cycle between a certain SOC range is usually employed to study this correlation. However, this method necessitates a lengthy period, running from months to years, prolonging the research duration significantly. The aging mechanisms obtained through this method are a result of the coupling of various SOC levels; the aging mechanisms at a specific SOC level are not accurately decoupled and analyzable. The proposed Zero-sum pulse method, using symmetrical pulses with small SOC amplitude variations on SOC, can explore aging mechanisms of LIBs at a specific SOC level and reduce the time to less than a week, which significantly expedite the research process. The aging mechanisms at 30%, 50%, 70%, and 90% SOC levels are explored to verify the accuracy and timeliness of this method.

INTRODUCTION

In recent years, lithium-ion batteries (LIBs) have increasingly been utilized as a renewable energy source. Their applications span a wide range of devices, including mobile phones, laptops, energy storage power stations, and Battery Electric Vehicles (BEVs).[1] However, researchers have not yet got a thorough understanding of the aging mechanisms of LIB due to the diversity of electrochemical reactions involved, which continue to hinder the further development and usage of battery in a wider range of scenarios.

Many possible battery degradation modes have been reported in literatures for various battery chemistries. It is frequently observed in the literature that the aging mechanisms in LIBs are typically categorized into three primary degradation modes: loss of lithium inventory (LLI), loss of active material (LAM), and conductivity loss (CL).[2–10] In addition to these primary aging mechanisms, concurrent aging-related side reactions also occur. These reactions are time-varying and nonlinear, adding another layer of complexity to the understanding of battery aging. Furthermore, the unique aging characteristics of different LIBs, which result from their distinct chemistries, increase the difficulty in comprehending general aging mechanisms.

Two main phenomena in LIBs contribute to LLI.[11] One is the cracking and regeneration of the solid electrolyte interphase (SEI). The SEI film plays a pivotal role in the functionality of LIBs. This film forms on the surface of the anode material during the initial charge and discharge cycle of a LIB.[5,12] The formation of the SEI film depletes nearly 10% of lithium ions, leading to irreversible capacity fade and reduction of charge and discharge efficiency of the electrode material. The other phenomenon that contributes to LLI is the formation of lithium dendrites, which is caused by lithium plating, i.e., not all precipitated lithium metal during discharge process is oxidized back into lithium-ion, but tends to form dendrites on the anode surface instead. These dendrites can grow until piercing through the SEI film, causing the SEI film to consume lithium ions to reconstruct.[13] Researchers have studied the factors that affect the cracking and regeneration of the SEI film, as well as the formation of lithium dendrites.[11,14,15] They found that the SEI film decomposes and regenerates more frequently under high temperature, which is attributed to the poor thermal stability of the organic components within the SEI film.[16,17] Meanwhile, low temperature facilitates the growth of lithium dendrites due to the kinetic instability of solvent molecules and electrolytes.[18] What is more, overcharging, which indicates a battery continuing to charge beyond its cut-off voltage, increases the overpotential across the anode resistance and reduces the anode potential to a value less than 0 V (relative to Li/Li^+), causing lithium ions to plate on the graphite anode instead of intercalating into it.[19] In addition, when a battery operates under high C-rate charging, the diffusion rate of lithium ions in the solid phase is slower than the electrochemical reaction rate. This results in a higher surface diffusion rate of lithium ions compared to the internal diffusion rate, leading to the plating of lithium ions on the anode surface.[20]

[1]Hubei Key Laboratory of Advanced Technology for Automotive Components, Wuhan University of Technology, Wuhan 430070, P.R. China
[2]Hubei Collaborative Innovation Center for Automotive Components Technology, Wuhan 430070, P.R. China
[3]School of Information Engineering, Wuhan University of Technology, Wuhan 430063, China
[4]School of Automation, Wuhan University of Technology, Wuhan 430070, China
[5]State Key Laboratory of Maritime Technology and Safety, Wuhan University of Technology, Wuhan 430070, P.R. China
[6]Lead contact
*Correspondence: wysh@whut.edu.cn (Y.W.), jingvwang@whut.edu.cn (J.V.W.)
https://doi.org/10.1016/j.isci.2024.110287

The primary indicators of LAM are graphite exfoliation, transition metal dissolution, and structural disordering. These factors contribute to capacity and CL. The performances of $LiFePO_4$ material and the electrolyte are adversely affected by high temperatures.[17] At elevated temperatures, the decomposition of the electrolyte, specifically PF_5, markedly increases. This reaction of PF_5 with H_2O leads to the production of hydrofluoric acid (HF), which reacts with the cathode material to form spherical particles, thereby leading to structural disordering.[21] It was discovered that traces of HF in the electrolyte can cause the disproportionation of Mn^{3+} into Mn^{2+} and Mn^{4+}, which results in the dissolution of the cathode electrode metal from the lattice into the electrolyte.[22] Consequently, cation contaminants such as Mn, Co, and Fe are deposited on the anode electrode surface. When the discharge rate exceeds 3C, it has a detrimental effect on the graphite anodes.[23] This leads to active material peel off from the battery electrode and a rapid increase in internal resistance, which in turn results in LAM and CL.

Copper dissolution, aluminum corrosion, binder decomposition, and cracking are the signatures of CL.[24] It found that during over-discharging, the Cu foil is initially oxidized to Cu^+ and Cu^{2+}.[25] These cations then diffuse from the anode side to the cathode side, where they are reduced back to metallic Cu. This process is triggered when over-discharging causes the potential of the graphite anodes to rise rapidly above the oxidation potential of Cu (3.92 V), leading to copper dissolution. Overcharging, on the other hand, causes the graphite anodes to expand. The resulting mechanical stress leads to binder decomposition and cracking of the current collector, which in turn causes CL.

During the charging and discharging process of LIBs, a voltage plateau is produced by the open circuit voltage (OCV) of the battery, which is due to the equilibrium state of the internal chemical reaction. The method of the incremental apacity (IC) curve analysis can convert this voltage plateau into a peak value, thereby providing an *in situ*, non-destructive method for analyzing the health status of the battery. A study by Yu et al.[26] presents a method for estimating the SOC of a battery based on the IC curve, particularly at high charging currents. The method involves deriving SOC-IC functions that use the measured IC value to estimate the battery's SOC. The effectiveness of the proposed method is validated using various charging currents and battery packs with different numbers of batteries. Electrochemical impedance spectroscopy (EIS) is a potent tool frequently employed to examine electrochemical processes in LIBs.[27,28] The Battery management system (BMS) typically monitors battery aging using capacity and power fade as indicators, as suggested by a study by Pastor-Fernández et al.[24] However, these two indicators fail to pinpoint the primary root causes of battery aging. Therefore, the use of EIS presents a novel approach to identify and quantify aging mechanisms over time.

Various aging mechanisms under diverse operation conditions have been studied as shown previously. In the studies of battery operation conditions, factors such as temperature, overcharging, over-discharging, and high rate charging and discharging have been given more attention than the operation conditions under various SOC ranges. Relatively few studies have explored the relationship between SOC ranges and aging mechanisms. Wikner and Thiringer[29] research the impact of aging under various SOC ranges for an electrified vehicle; the experiment was conducted for 3 years. The battery cycled 8,000 times in the 10–20% SOC range and still does not reach 80% state of health (SOH).[30,31] Long-term cycles prolong the period of research significantly. At the same time, many of them focus solely on the influence of SOC ranges on aging mechanisms. These articles usually put some SOC levels together to form an SOC range, so the characteristics of aging mechanisms are the result of coupling of some SOC levels. Almost no research investigates the process of aging mechanisms deeply at a specific SOC level. Thus, a comprehensive understanding of the exact aging mechanisms associated with a specific SOC level remains elusive. The Zero-sum pulse test method proposed in the work can explore the aging mechanisms of LIBs at a specific SOC level. The aging mechanisms at 30%, 50%, 70%, and 90% SOC levels are explored to verify the accuracy and timeliness of this method.

The remainder of this paper is organized as follows. The part of the zero-sum pulse test method illustrates the theory of the Zero-sum pulse method. The part of the experiments and theory outlines the procedure of the Zero-sum pulse test under different SOC levels and other tests. The part of the results and discussion presents the results of the Zero-sum pulse test, the analyzation from IC curve, and EIS as well as the result of battery disassembly. The part of the conclusion summarizes the conclusions and the novelty of this paper.

ZERO-SUM PULSE TEST METHOD

The Zero-sum pulse is characterized by a high-rate symmetric charging and discharging current pulse. As shown in Figure 1A, the total current applied during both charging and discharging is equal, which implies that the net charging capacity is zero throughout the pulse. Consequently, capacity should remain constant before and after the pulses. Figure 1B is the diagram with parasitic reactions; it consumes a part of the applied current and makes capacity loss when parasitic reactions occur under the charging pulse conditions. This results in a lower amount of current being used for the practical charge. Therefore, the existence of parasitic reactions causes the capacity to be lower than it was before the Zero-sum pulse. V_1 and V_2 represent the voltage of a cycle without parasitic reactions, while V_3 and V_4 represent the voltage of a cycle with parasitic reactions. It is evident that V_4 does not equal V_1 due to the presence of parasitic reactions, which also results in a loss of applied current and capacity.

When a battery operates within SOC ranges, the capacity loss incurred is the sum of the losses at each SOC level. This makes it challenging to determine the exact capacity loss at each SOC level and to identify which aging mechanism is triggered at a specific SOC level. The Zero-sum pulse method offers the two advantages; one is enabling the battery to undergo hundreds of repeated Zero-sum pulse cycles at a given SOC level. This allows for the accumulation of all external characteristics of an aging mechanism, such as voltage decrease, resistance increase, and capacity loss. The other is short period of time, time that battery operates within SOC ranges is the sum of time at each SOC

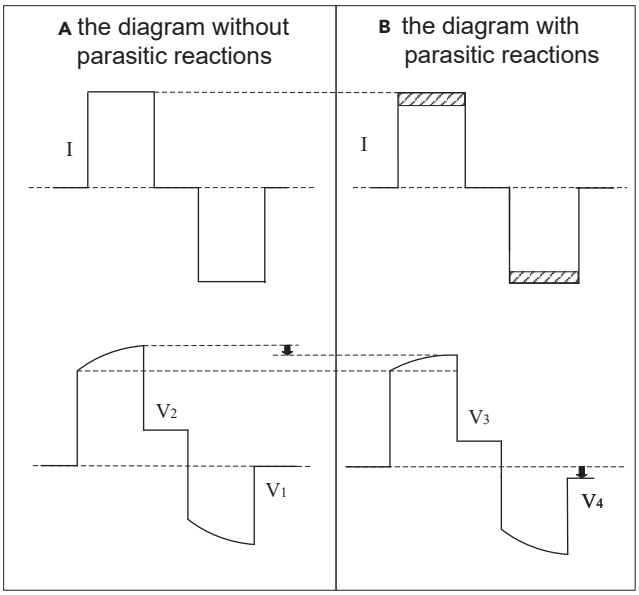

Figure 1. The theory of the Zero-sum pulse test method

level; thus, time is short when battery cycles under a specific SOC level. Therefore, the Zero-sum pulse testing method allows for the analysis of these aging mechanisms at a specific SOC level.

EXPERIMENTS AND THEORY

To investigate the relationship between different SOC levels and aging mechanisms, after passing the capacity and resistance conformance test, we selected 10 commercial 18650 $LiFePO_4$ power batteries from the same batch as our test subjects. In order to avoid the accidental error and guarantee the reliability of results, these batteries were equally divided into five groups, with their parameters summarized in Table 1. A NEWARE CT-4008-5V-12A battery test equipment was employed to test the batteries under different SOC levels. Throughout the testing process, the ambient temperature was maintained around 25°C.

Reference performance test

We conducted a reference performance test (RPT) on the 10 batteries. The RPT consisted of three main tests: a 1/3C rate nominal capacity test, a 1/20C rate capacity test, and a hybrid pulse power characterization (HPPC) test. The 1/3C rate nominal capacity test included an initial capacity test, an end capacity test, and 8 times capacity tests that were performed regularly after every 500 Zero-sum pulses. The object of the initial and end capacity test is to acquire capacity before and after the Zero-sum pulse test, and the aim of the 8 times capacity test during experiment is to recalibrate the capacity per cycle so that make the battery operate at the target SOC level. The initial capacity test, conducted prior to the implementation of the Zero-sum pulse testing method, involved three full charging and discharging cycles. Each cycle included a 1/3C rate constant current-constant voltage (CC-CV) charging and a 1/3C rate constant current (CC) discharging. Six hours following the Zero-sum pulse testing, an end capacity test was conducted. The procedures for the end capacity test and the 8 times capacity tests were identical to the initial capacity test. The 1/20C rate capacity test aimed to acquire the maximum available capacity and to calculate the IC curve and the OCV-SOC curve. The process for this test was similar to the 1/3C rate nominal capacity test. The HPPC test was designed to measure the ohmic resistance to verify the conformance of the battery, which guarantee the tested battery have a great consistency before experiments. The entire experimental process is depicted in Figure 2.

Zero-sum pulse test

The voltage, current, and capacity were measured every second by the NEWARE CT-4008-5V-12A battery test equipment during the experiment. The particular processes of the Zero-sum pulse testing method are shown in Table 2. Each group was charged to SOC levels of 30%, 50%, 70%, and 90% by step 1, respectively. A 4C charging and discharging pulse was maintained for a duration of 18 s, which represents 2% of the total capacity. Thus, it can be seen that battery operates at a specific SOC level. Steps 1–4 consisted of a cycle and steps 3–4 are repeated 500 times per cycle. Steps 5–7 were used for capacity calibration per 500 Zero-sum pulses to rectify the deviation of capacity caused by the aging at a given SOC level, and the cycle was carried out a total of 8 times. Figure 3 shows the experimental voltage curve and the partial enlarged detail of the Zero-pulse test. The battery, through the process described previously, can maintain stable operation at a specified SOC level. Moreover, the external aging characteristics observed at this specific SOC level can be interpreted as the result of the aging mechanism activated at that particular SOC level.

Table 1. Specifications of battery under test

Items	Parameter
Cathode material	$LiFePO_4$
Anode material	Graphite
Nominal capacity (mAh)	2000
Charging cut-off voltage (V)	3.6
Discharging cut-off voltage (V)	2.5
Maximum charge and discharge ratio (C)	5

The IC curves

The 1/20C rate capacity test in the RPT aimed to acquire the maximum available capacity and to calculate the IC curve. The peak value of the IC curve is indicative of changes in the voltage platform. When the battery operates at a voltage platform, it maintains a constant charging current. Despite the increase in charging capacity, the battery voltage remains unchanged. This implies dV is small when the dQ changes, resulting in a large dQ/dV value. The flatter the voltage platform of the battery, the larger the peak of the IC curve becomes. The calculated formula of the IC (Equation 1) is used:

$$IC = \frac{dQ}{dV} = \frac{I\Delta t}{\Delta V} \quad \text{(Equation 1)}$$

where dQ is the amount of current (I) accumulated at each sample time point and ΔV is the change of the terminal voltage between two sample time point.

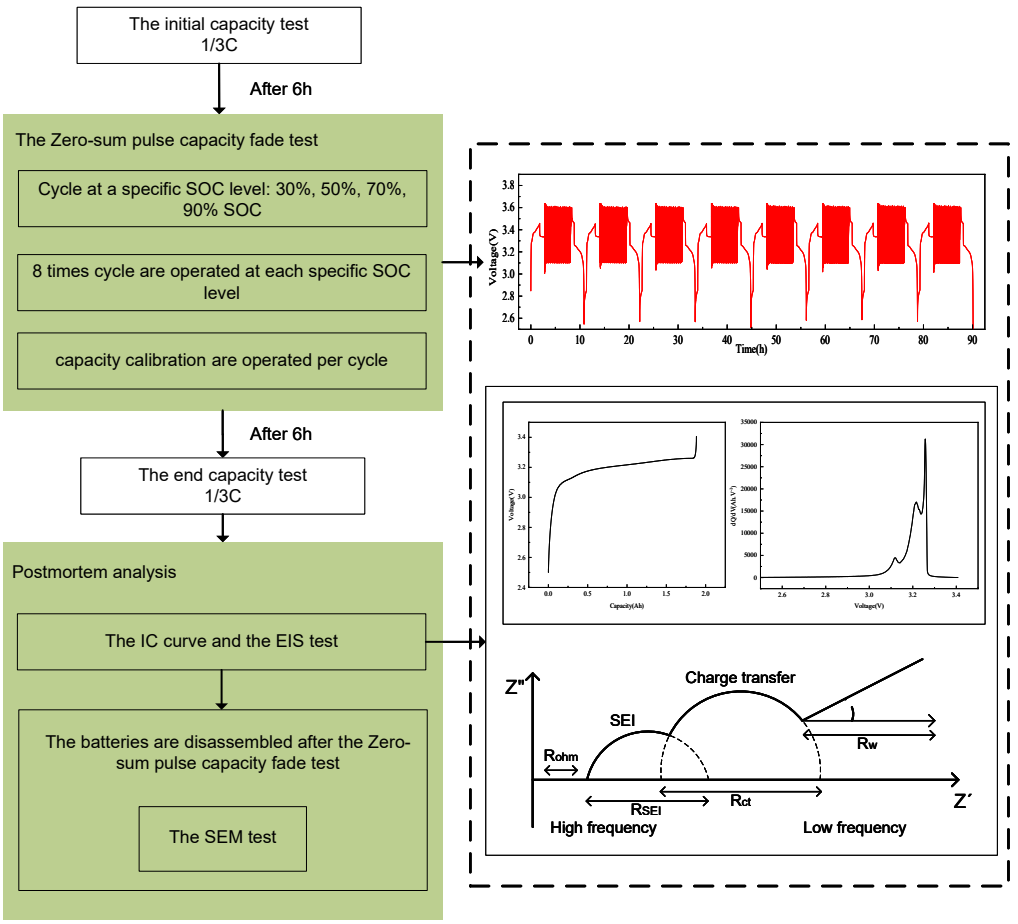

Figure 2. The whole experiment procedure diagram

Table 2. The particular processes of the Zero-sum pulse testing method

Step	Condition	Cut-off condition
1	1/3C-charge	Target SOC level
2	Rest	3h
3[a]	4C-charge pulse	18s
4[a]	4C-discharge pulse	18s
5	1/3C-charge	3.6V
6	Rest	1h
7	1/3C-discharge	2.5V

[a]Step 3 and step 4 are repeated 500 times per cycle.

The IC curve for the graphite anode exhibits five peaks, each corresponding to a phase transformation process of the graphite (C_{72}, C_{36}, C_{18}, C_{12}, and C_6). However, only three of these peaks are discernible in Figure 4. The positive electrode undergoes a transformation between $FePO_4$ and $LiFePO_4$. This transformation process corresponds with the phase change process, which encompasses the single-phase solid-state dissolution reaction stage and the pseudo-binary stage of Li_xFePO_4 to $Li_{1-y}FePO_4$. The single-phase solid-state dissolution reaction stage is referred to as stage I, and the pseudo-binary phase transition, which involves a battery voltage plateau stage with a potential capacity change exceeding 95%, is referred to as stage II. Consequently, the three peaks of the anode are named 1*II peak, 2*II peak, and 5*II peak, respectively.[32,33] Dubarry et al.[6] suggested that 1*II peak and 2*II peak represent the phase transition process of active materials. A larger quantity of active materials can lead to a more intense reaction and potentially a larger corresponding peak value. Therefore, decline in the y axis of the IC curve are regarded as LAM. According to Ohm's law, the terminal voltage equals the electric potential minus the internal resistance times the current. As the ohmic internal resistance increases with the aging process, the corresponding voltage decreases. This is manifested as a shift toward terminal voltage reduction in the IC curve.[34,35] Thus, the offset of the IC curve in the horizontal coordinate direction is used to analyze ohmic internal resistance. Ohmic internal resistance increase can be used as an indicator of the CL.[4] Thus, by analyzing changes of peaks and the corresponding terminal voltage decrease, LAM and CL of the battery are analyzed. The Equations 2 and 3 are used to quantify the aging process of LAM and CL, respectively.

$$LAM = \frac{abs\left(max\left(\frac{dQ}{dV}\right)_i - max\left(\frac{dQ}{dV}\right)_{d-soc}\right)}{abs\left(max\left(\frac{dQ}{dV}\right)_i\right)} \quad \text{(Equation 2)}$$

$$CL = \frac{max\,(V_i) - max\,(V_{d-soc})}{max\,(V_i)} \quad \text{(Equation 3)}$$

where i represents the initial IC curve and d-soc indicates the different SOC levels. The Equations 2 and 3 are used to quantify the aging process under different SOC levels based on the IC curve.

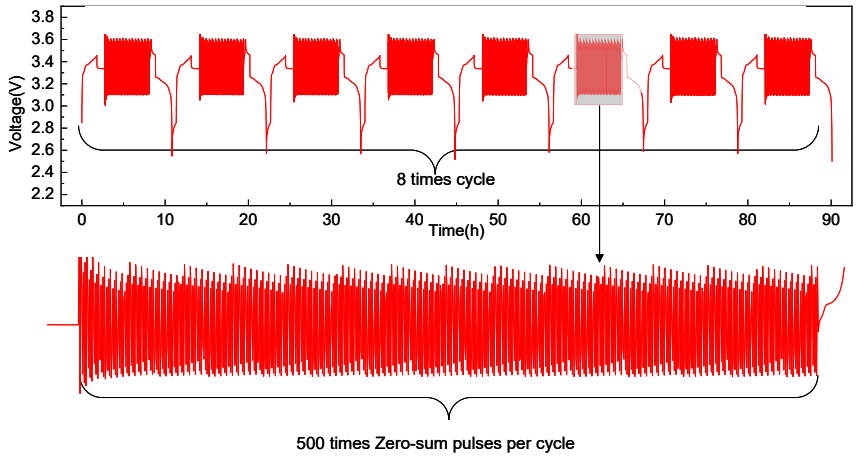

Figure 3. The experimental voltage curve and the partial enlarged detail of the Zero-pulse test

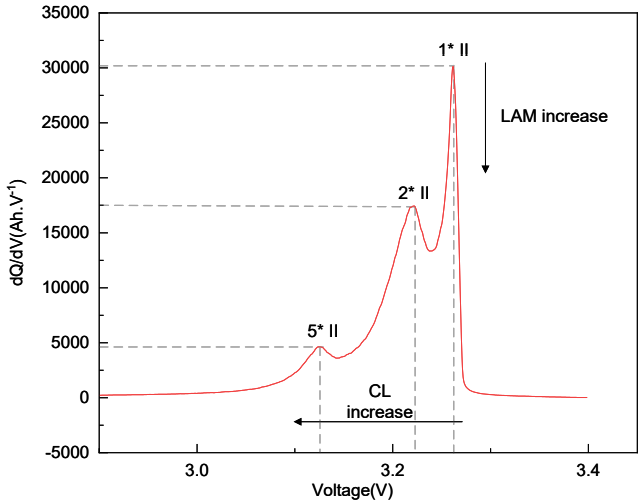

Figure 4. The IC curve of the $LiFePO_4$ battery

The EIStest

The EIS is a commonly employed experimental method for obtaining a more profound understanding of the electrochemical processes in battery. In parameters setting of EIS test, the amplitude is 0.005 V, high and low frequencies are 100,000 Hz and 0.001 Hz, respectively. The EIS test data are depicted via the inverse of Nyquist plots generally. These plots correlate the imaginary part of the impedance (y axis) with its real part (x axis), as illustrated in Figure 5. Different frequencies in EIS can represent various aging mechanisms of a battery. The standard EIS contains some parameters in the following. One parameter is the ohmic resistance, denoted as R_{ohm}. It represents the impedance of electron motion in the current collectors and electrolyte.[24,36] Two semicircles shown in Figure 5 that are plotted with brown line; the first semi-circle is interpreted as the phenomenon of lithium-ion migration through the SEI film, denoted as R_{SEI}. This resistance reflects the impedance encountered by lithium-ions passing through the SEI film. The formation of the SEI film results in the consumption of lithium ions. Concurrently, the expansion of the graphite anode, triggered by the intercalation and deintercalation of lithium ions, leads to the cracking of the SEI film. This cracking prompts the SEI film to consume a portion of the applied lithium ions for its regeneration and repair, resulting in a thicker film and increased resistance. Consequently, the increase of R_{SEI} serves as an indirect representation of the LLI. The second semi-circle in the middle frequency range is associated with the charge transfer resistance, denoted as R_{ct}. It represents the impedance encountered during electrochemical reactions.[36] Apart from the SEI film, effects such as dendrite growth or micropore clogging are primarily due to LLI. These effects result increase of resistance in the electrochemical reactions. Therefore, the increase in R_{ct} is also a sign of LLI. The straight line in the low-frequency range is associated with the impedance of diffusion in the graphite,[37] referred to as Warburg impedance (R_w). Similarly, the expansion and shrinkage of the graphite anode due to the intercalation and deintercalation make active material crack as well, and can even result in graphite exfoliation and structural disorder. As a consequence, the diffusion rate of lithium ions in the active material decreases, which is indicative of an increase in impedance. Therefore, an increase in R_w serves as an indicator of LAM. The Equations 4, 5, and 6 are used to quantify the aging process of LAM and LLI, respectively.

$$CL = \frac{R_{ohm,d-soc} - R_{ohm,i}}{R_{ohm,i}} \quad \text{(Equation 4)}$$

$$LLI = \frac{(R_{SEI,d-soc} - R_{SEI,i}) + (R_{ct,d-soc} - R_{ct,i})}{R_{SEI,i} + R_{ct,i}} \quad \text{(Equation 5)}$$

$$LAM = \frac{R_{w,d-soc} - R_{w,i}}{R_{w,i}} \quad \text{(Equation 6)}$$

where i represents the EIS curve of the initial EIS curve and d-soc indicates the different SOC levels. The Equations 4, 5, and 6 are used to quantify the aging process under different SOC levels based on the EIS.

A postmortem study

After all tests, batteries are disassembled within an argon-filled glovebox and anode samples are collected. The anode materials are then soaked in dimethyl carbonate (DMC) for 2 h to eliminate the influence of the electrolyte. Afterward, the samples are dried using a vacuum drying oven at 100°C for 10 h. Finally, the surface morphology of the anode material is observed using SEM.[38–41]

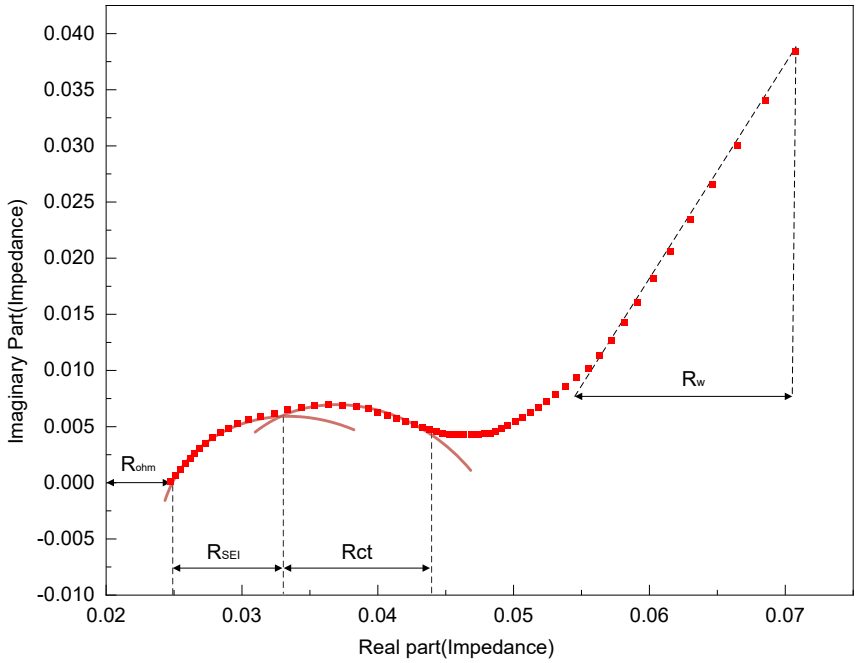

Figure 5. The EIS spectrum

RESULTS AND DISCUSSION

The discussion of the Zero-sum pulse testing method

Figure 6 depicts the state of capacity fade after the 800 Zero-sum pulses test. The battery of the first group underwent a full charging and discharging cycle, henceforth referred to as the general battery. The general battery operates from 0% to 100% SOC; thus, the aging of this battery is a comprehensive result by various aging mechanisms. To clearly elucidate the aging mechanisms occurring at specific SOC levels, the general battery is used as a reference. By comparing the general battery with batteries cycled at various SOC levels, we can isolate the aging mechanisms that occur at an individual SOC level from that in the general battery. Due to the general battery undergoing the full charging and discharging cycle and other batteries charging and discharging at a specific SOC level, these batteries cannot be compared on a timescale. Thus, the Ampere-hour throughput is used as the horizontal axis[42]; i.e., the batteries that operate at a specific SOC level charge capacity per one Zero-sum pulse cycle is 22 Ah, and the general battery charge capacity at full charging and discharging cycle is 2 Ah, only 11 cycles on the general battery can be correspond to one Zero-sum pulse cycle on other batteries. The y axis represents the coulombic efficiency (CE). CE is depicted in the following Equation 7.

$$CE = \frac{Q_{discharge}}{Q_{charge}} \quad \text{(Equation 7)}$$

In the above formula, Q_{charge} represents the charge capacity from the initial capacity test, is discharge capacity sampled once every 500 Zero-sum pulses. Thus, through the CE and ampere-hour throughput, a uniform standard platform has been established for further analysis by the five groups. It is observed that the CE of the general battery, as well as the batteries with 50% and 70% SOC, almost shows a linear attenuation. It illustrates that the respective aging system remains unchanged throughout the cycle in these three testing conditions.[14,43] However, this does not imply that the same aging mechanisms are observed in the general battery, the battery with 50% SOC, and the battery with 70% SOC.

Obvious CE degradation occurs in the battery with 30% and 90% SOC, which shows non-linear attenuation. Non-linear attenuation implies that the inner aging system has altered during the test in these two test conditions.[44] The battery with 30% SOC exhibits a slow value of CE (around 98%) in the first 400 cycles, and accelerated degeneration happen between 400 and 600 cycles, which decrease from 98% to 96%. This means that the emergence of a new aging mechanism in the aging system or the degree of an existing aging mechanism increases, resulting in an increase in lithium-ion consumption. The value of CE is always around 96% in last 200 cycles that means the CE degradation slows down again in the last cycles. In the battery with 90% SOC, the value of CE is very slow (about 97%) in first 300 cycles. It degrades faster between 300 and 500 cycles, which decline from 97% to 92%. The sudden CE degradation illustrates that the internal aging system changes in the battery with 90% SOC, which means that the appearance of more new aging mechanisms consumes more lithium-ion or the degree of existing aging mechanisms deepen even more. The conclusions analyzed above illuminate that there are different CE degradations at diverse SOC levels in the same ampere-hour throughput, which illustrate that the aging system at various SOC levels are different.

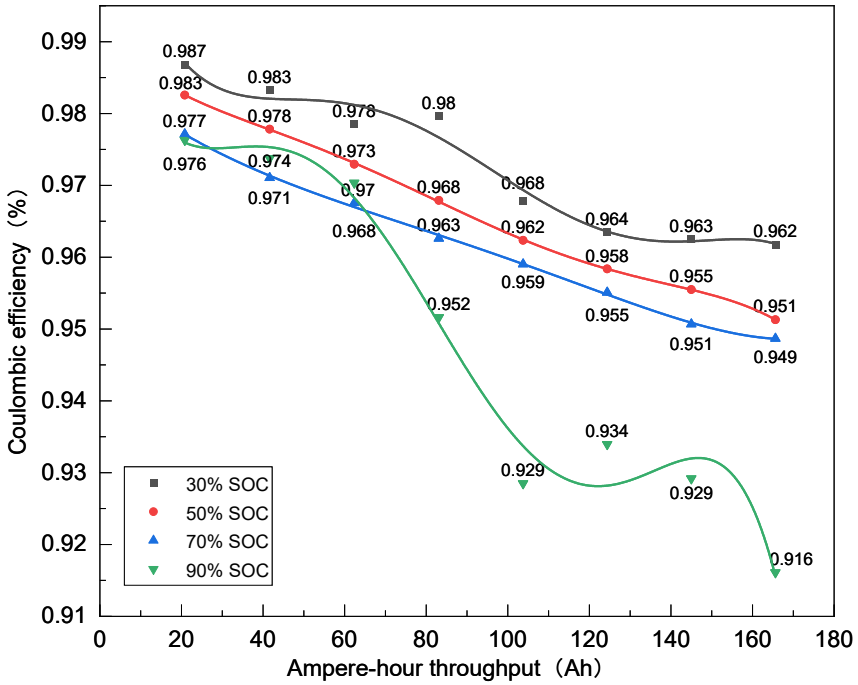

Figure 6. The degradation of CE curve through the Zero-sum pulse test

Table 3 shows the capacity of batteries in the initial and end capacity test, as well as the difference values between them. The initial capacity test is taken before the Zero-sum pulse testing method, and the end capacity test is collected after the Zero-sum pulse. Each group of batteries exhibits a different degree of capacity degradation. XX%-1 and XX%-2 are two batteries from same group that suffer the same aging condition to guarantee the reliability of results. By analyzing Table 3, the values of the capacity attenuation are nearly identical in each group, and increases gradually with the increment of SOC, which illuminate that the aging systems are different at various SOC level and the new aging system are formed at high SOC period, causing the capacity plunge at 90% SOC level. The specific aging system need to be analyzed further by the IC and EIS in the next work.

Analysis of the IC curve

The IC curve is utilized to describe the LAM and CL of all batteries after the Zero-sum test. Figure 7A displays the IC curves of batteries with various SOC levels. Prior to the Zero-sum pulses test, a 1/20C rate capacity test is performed to acquire the initial IC curves of all batteries. These initial IC curves are intended for comparison with the IC curve after degradation. Given the favorable consistency among the batteries, their initial IC curves are similar. Therefore, a single initial IC curve is presented as representative of all initial IC curves. It can be seen that among all curves, 1*II and 2*II peak values of the initial IC curve are the highest. The 1*II and 2*II peak values decrease gradually with the growth of SOC levels, this means LAM increases gradually with the increase of SOC levels, and the LAM of the battery at 90% SOC level is the most serious. It is interesting that the 1*II peak value of the battery at 30% SOC level on abscissa is less than that at 50% and 70% SOC levels and the general battery as shown in Figure 7B.

In order to study further, aging mechanisms are quantified by the variation in the horizontal and vertical coordinates of each curve on the IC curve.[4] The Equations 2 and 3 mentioned previously are used to quantify the aging process of the LAM and CL, respectively. The calculated data are shown in Table 4.

According to the results of IC curve data quantization, the tendency of LAM and CL with the growth of SOC levels are shown in Figure 8. CL in the battery with 30% SOC level is greater than the battery with 50% and 70% SOC level, but the LAM at 30% SOC level is the lowest, which means the main reason of the enhancement in CL is not caused by the LAM, but others. In addition, the CL at 50% and 70% SOC level are relatively low, but the LAM at 70% SOC level appear to jump compared with that of 30% and 50% SOC levels, and the LAM at 90% SOC level is highest. It illuminates that LAM has become the dominant aging mechanism at a high SOC level, which leads the CL growth caused by the LAM.

Analysis of the EIS

The EIS curve is utilized to describe the LAM, LLI, and CL, due to the EIS test being easily affected by the poor connections or contact, which makes the EIS test system inaccurate. The result of high frequency as shown in Figure 9 is irregularity, thus CL is no longer analyzed in the EIS curve. Due to the proximity of the curves to each other, it is challenging to analyze the aging mechanisms in detail. Therefore, Figure 10

Table 3. Capacity analyses of all batteries

	Value(mAh)		
Condition	Initial capacity	End capacity	Capacity attenuation[a]
General-1	1878.5	1871.6	6.9
General-2	1882.3	1875.1	7.2
30%-1	1897.6	1893.8	3.8
30%-2	1880.9	1878.3	2.6
50%-1	1880.7	1867.2	13.5
50%-2	1895.0	1881.1	13.9
70%-1	1879.7	1865.2	14.5
70%-2	1883.4	1867.8	15.6
90%-1	1900.5	1809.2	91.3
90%-2	1897.6	1804.7	92.9

[a]Value of capacity attenuation is the initial capacity minus the end capacity.

presents a data quantization diagram of the EIS curve. The calculated data are shown in Table 5. The Equations 5 and 6 mentioned previously are used to quantify the aging process of the LLI and LAM, respectively.

It is clearly indicated that the LLI is the highest and the LAM is the lowest at 30% SOC level compared with LLI and LAM at other SOC levels, which is 90.52% and 19.64%, respectively. The CL of 30% SOC level is 0.11%, which is relatively higher than that at 50% and 70% SOC levels in Figure 8. Thus, it can be concluded that the main reason is that it took place the SEI film fracture and formation. More lithium ions take part in the reaction of the SEI film formation and regenerate, which causes capacity fade (CE decrease) and more CL.[45] With the increment of SOC level, LLI caused by the SEI film decrease gradually, moving from 90.52% to 12.22%. However, LAM increased step by step, transitioning from 19.64% to 41.82%, which the tendency consistent with the results in Figure 8, indicating that the dominant aging mechanism has changed from LLI to LAM with the increase of SOC level. The reason for LAM becoming the main aging mechanism at high SOC is the greater strain caused by larger expansion of the negative electrode. The great strain makes electrode material crack severely, for example, graphite exfoliation and structural disordering of the electrode material leads to less active material work normally.

The LLI at 90% SOC is bigger than that at 50% and 70% SOC. The primary reason is the great expanded strain not only makes electrode material crack severely, but also make the SEI film swell even more,[46] which caused the SEI film to fracture seriously. More lithium ions are used to repair the SEI film; thereby, the LLI rises again, and growth of the SEI film makes the film thicker, causing the increase of internal resistance,[47] thus, the corresponding CL at 90% SOC level is large, as shown in Figure 8.

The result of battery disassembly

The morphologies of anode material are inspected through SEM, which is shown in Figure 11. Figures 11A–11E show the microstructures of all batteries after the Zero-sum pulse test. Figure 11A shows the graphite particles on the anode surface are evenly distributed, and they are almost whole and barely broken. More graphite particles are broken with the increase of SOC. This is because more lithium ions are inserted into the anode material with the increase of SOC, which caused strain expands gradually. Therefore, with the increase of SOC, more active materials are broken and pulverized, as shown in Figures 11B–11E. The cracking of the battery with 90% SOC is the most serious. Conducting that LAM is the main aging mechanism at high SOC, which the conclusion identical to the EIS analysis.

Meanwhile, some lithium dendrites (white spot) had appeared on the surface of anode material in the battery with 30% SOC, and the situation is worse in the battery with 50% and 70% SOC. It is evidence that the lithium dendrites in the battery with 30%, 50%, and 70% SOC are less than that in the battery with 90% SOC; and there are some areas of lithium dendrites that are already formed in the battery with 90% SOC, which cause further LLI at 90% SOC. The conclusion is consistent with the Figure 10.

Conclusion

In this study, the relationship between the aging mechanisms and SOC level is explored in 18650 batteries. The Zero-sum pulse test is proposed to investigate the aging mechanisms of $LiFePO_4$ batteries at a given SOC level, which can decouple the aging mechanisms that occur at an individual SOC level from the overall aging mechanisms that occur between a certain SOC range. Meanwhile, the method can obtain substantial results with drastically reduced test time. This method is utilized to conduct research of aging mechanisms at four different SOC levels: 30%, 50%, 70%, and 90%. The RPT test was conducted and analyzed the results of the IC curve and the EIS curve quantitatively to delve deeper into the details of the aging mechanisms at various SOC levels. Finally, the results of the SEM verify the aforementioned analysis. The key conclusions from study are summarized as follows.

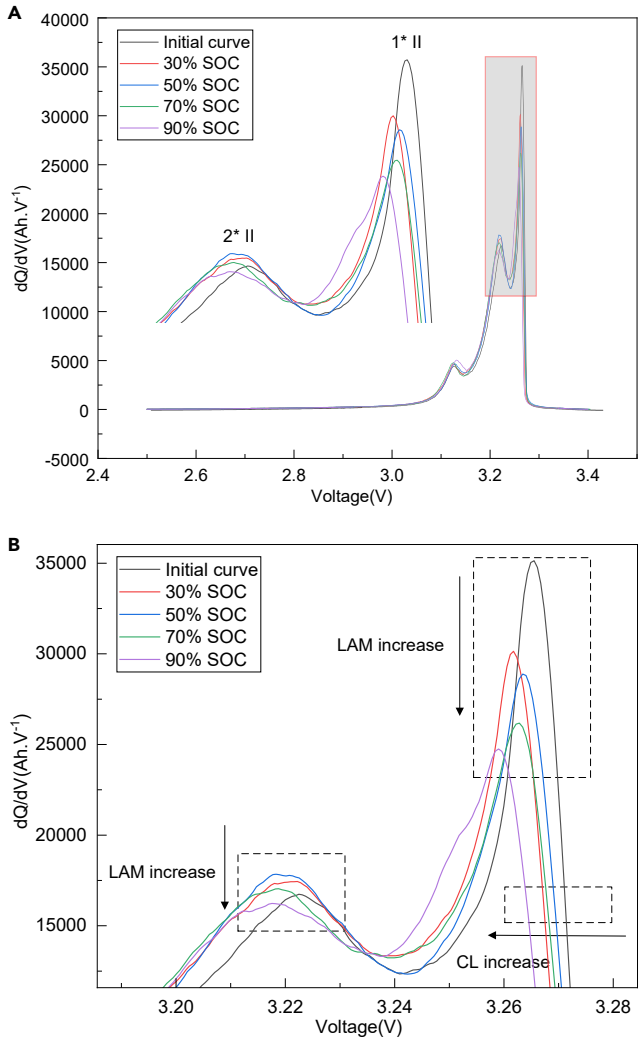

Figure 7. The IC curve

(A) Evolution of the IC curves of the batteries with 30%, 50%, 70% and 90% SOC levels.

(B) A partial enlarged view of the IC curve.

(1) The LLI that occurred at 30% SOC level is the highest compared with LLI at other SOC levels, and the CL is relatively higher than that at 50% and 70% SOC levels. It indicates that the main aging mechanism at low SOC is the LLI caused by the SEI film formation and regeneration. Based on the results, it can be suggested that LIBs should avoid operating at low SOC to reduce great capacity loss, extending the cycle lifetime of battery.

Tabel 4. The data analysis of the all batteries from the IC curve

Conditions	Values			
	$\max\left(\frac{dQ}{dV}\right)$	max (V)	LAM (%)	CL (%)
Initial IC curve	35140.19	3.2721		
30% SOC level	30140.51	3.2684	14.23	0.11
50% SOC level	28889.22	3.2705	17.79	0.05
70% SOC level	26180.38	3.2693	25.50	0.09
90% SOC level	24755.23	3.2657	29.55	0.19

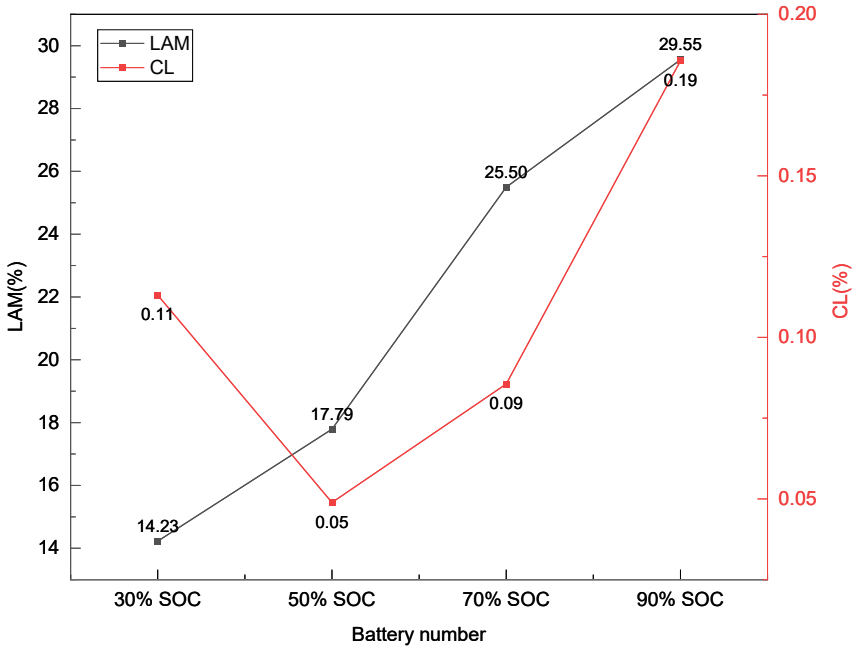

Figure 8. The tendency of LAM and CL with the growth of SOC

(2) The LLI, LAM, and CL of the battery at 50% and 70% SOC exhibit great performance retention, which are lower than that at 30% and 90% SOC. It indicated that severe battery aging mainly occurs at low and high SOC. Thus, operating battery under the intermedium SOC is an optimal choice for a long lifetime.

(3) The LAM that occurred at 90% SOC level is the highest compared with LAM at other SOC levels, and the LLI increased again at 90% SOC level. It suggests that the main aging mechanism is the LAM caused by larger expanded stress, and the graphite expansion caused by LAM will make the SEI film crack again at high SOC, after which the SEI film regenerate by consuming lithium ions. Thus, large capacity fade occurs at high SOC.

The aforementioned conclusions are consistent with previous results by Gao et al.[39] and Chowdhury et al.[48] It demonstrates that the Zero-sum pulse method can accurately decouple aging mechanisms at an SOC level from a broader SOC range. This method can significantly degrade a battery at a specific SOC level in less than a week. By coordinating with the IC curve and EIS curve, the Zero-sum pulse method enables effective and timely analysis of aging mechanisms at various SOC levels.

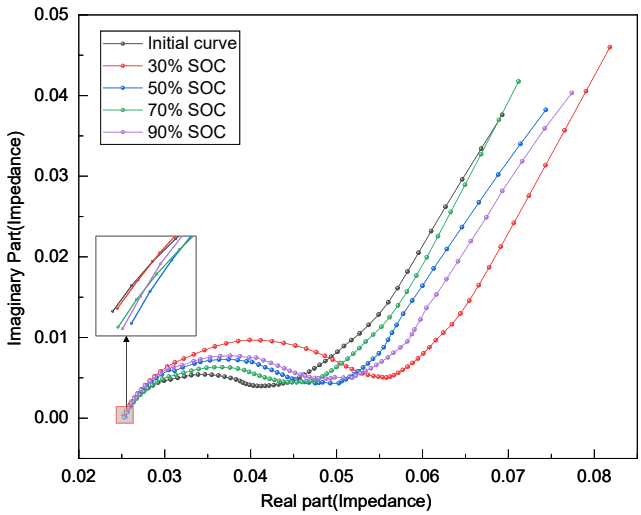

Figure 9. Evolution of the EIS curves of the general battery and the batteries with 30%, 50%, 70%, and 90% SOC level

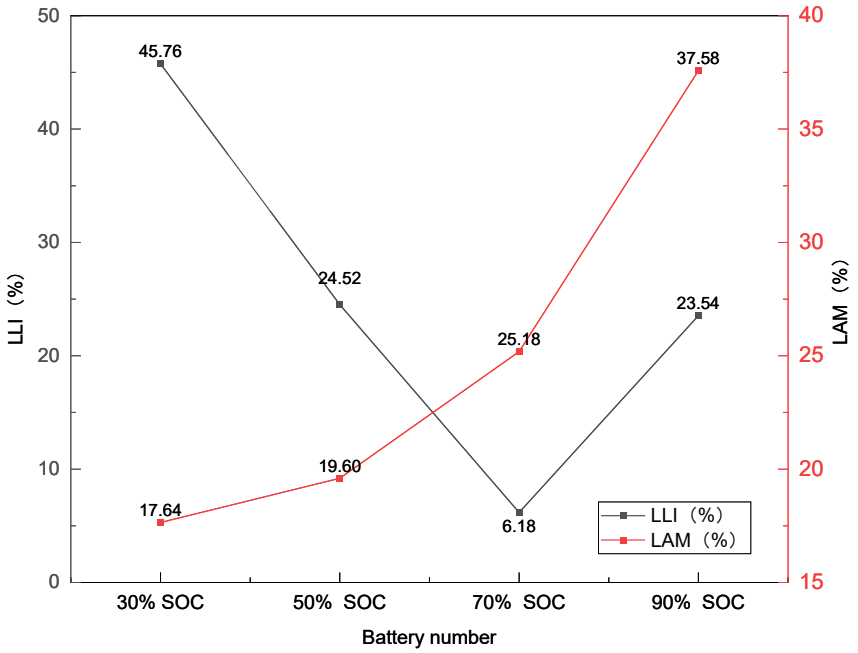

Figure 10. The tendency of LLI and LAM with the growth of SOC

Limitations of the study

This paper does not explore the aging mechanisms at different SOC levels under various temperatures. This will be the focus of our future works.

STAR★METHODS

Detailed methods are provided in the online version of this paper and include the following:

- KEY RESOURCES TABLE
- RESOURCE AVAILABILITY
  - Lead contact
  - Materials availability
  - Data and code availability
- METHOD DETAILS

ACKNOWLEDGMENTS

This work was supported by the National Natural Science Foundation of China under grants no. 52277224 and 51977163, and Science and Technology on Ship Integrated Technology Laboratory under grant No. 61422172320104.

Table 5. The quantified data of all batteries from the EIS curve

	Values			
Conditions	$R_{SEI}+R_{ct}$	R_W	LLI(%)	LAM(%)
Initial curve	16.04	20.59		
30% SOC level	30.56	24.63	90.52	19.64
50% SOC level	23.82	25.08	48.50	21.81
70% SOC level	18.00	26.36	12.22	28.02
90% SOC level	23.51	29.20	46.57	41.82

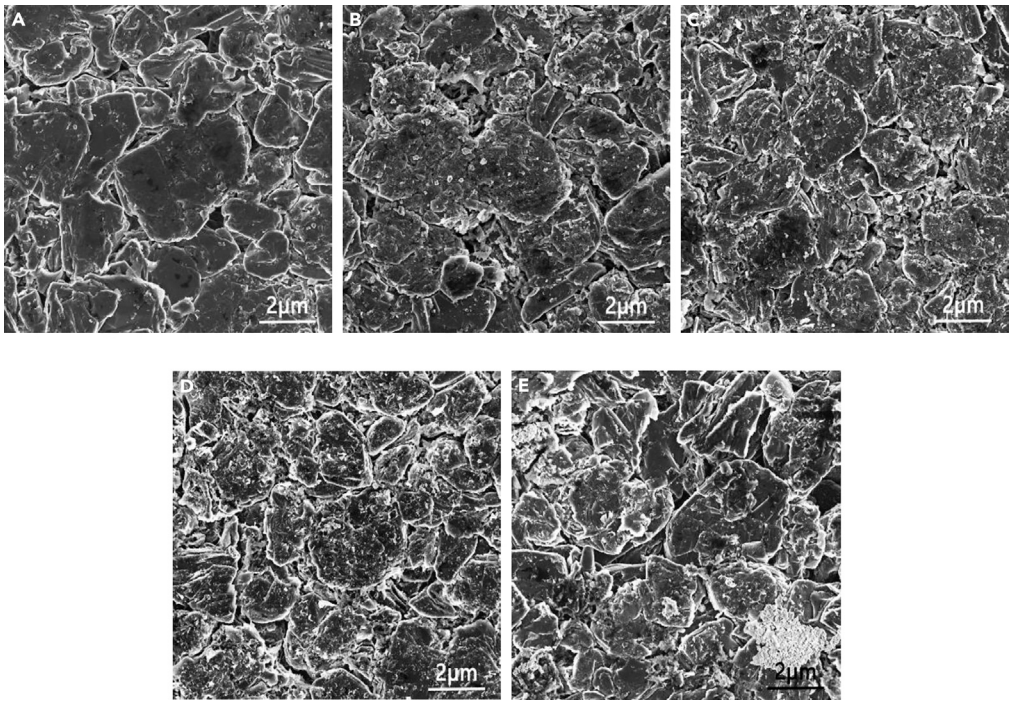

Figure 11. The morphologies of anode material

The microstructures of all batteries after the Zero-sum pulse test that cycle at (A) full charging and discharging, (B) 30% SOC, (C) 50% SOC, (D) 70% SOC, and (E) 90% SOC.

AUTHOR CONTRIBUTIONS

J.K: methodology, investigation, and supervision. G.Y: methodology, investigation, and writing – original draft. Y.W: supervision and writing – review & editing. J.V.W: supervision and writing – review & editing. Q.W.: writing – review & editing and investigation. G.Z: conceptualization and writing – review & editing.

DECLARATION OF INTERESTS

The authors declare no competing interests.

Received: March 30, 2024
Revised: May 9, 2024
Accepted: June 13, 2024
Published: June 17, 2024

REFERENCES

1. Goodenough, J.B., and Kim, Y. (2010). Challenges for Rechargeable Li Batteries. Chem. Mater. *22*, 587–603. https://doi.org/10.1021/cm901452z.
2. Zhang, Q., and White, R.E. (2008). Capacity fade analysis of a lithium ion cell. J. Power Sources *179*, 793–798. https://doi.org/10.1016/j.jpowsour.2008.01.028.
3. Dubarry, M., and Liaw, B.Y. (2009). Identify capacity fading mechanism in a commercial LiFePO4 cell. J. Power Sources *194*, 541–549. https://doi.org/10.1016/j.jpowsour.2009.05.036.
4. Pastor-Fernández, C., Uddin, K., Chouchelamane, G.H., Widanage, W.D., and Marco, J. (2017). A Comparison between Electrochemical Impedance Spectroscopy and Incremental Capacity-Differential Voltage as Li-ion Diagnostic Techniques to Identify and Quantify the Effects of Degradation Modes within Battery Management Systems. J. Power Sourc. *360*, 301–318. https://doi.org/10.1016/j.jpowsour.2017.03.042.
5. Agubra, V., and Fergus, J. (2013). Lithium Ion Battery Anode Aging Mechanisms. Materials *6*, 1310–1325. https://doi.org/10.3390/ma6041310.
6. Dubarry, M., Truchot, C., and Liaw, B.Y. (2012). Synthesize battery degradation modes via a diagnostic and prognostic model. J. Power Sourc. *219*, 204–216. https://doi.org/10.1016/j.jpowsour.2012.07.016.
7. Safari, M., and Delacourt, C. (2011). Aging of a Commercial Graphite/LiFePO4 Cell. J. Electrochem. Soc. *158*, A1123. https://doi.org/10.1149/1.3614529.
8. Wang, J. (2011). Cycle-life model for graphite-LiFePO4 cells. J. Power Sourc. *196*, 3942–3948.
9. Striebel, K., Guerfi, A., Shim, J., Armand, M., Gauthier, M., and Zaghib, K. (2003). LiFePO4/gel/natural graphite cells for the BATT program. J. Power Sourc. *119–121*, 951–954. https://doi.org/10.1016/S0378-7753(03)00295-7.

10. Ramadass, P., Haran, B., White, R., and Popov, B.N. (2003). Mathematical modeling of the capacity fade of Li-ion cells. J. Power Sourc. *123*, 230–240. https://doi.org/10.1016/S0378-7753(03)00531-7.
11. Zhengguo, W.U., Jianbo, Z.H., Zhe, L.I., and Yann, L.B. (2018). Aging abuse boundary of lithium-ion cell above room temperature. J Automot. Safety Energy *9*, 99–109.
12. Verma, P., Maire, P., and Novák, P. (2010). A review of the features and analyses of the solid electrolyte interphase in Li-ion batteries. Electrochim. Acta *55*, 6332–6341. https://doi.org/10.1016/j.electacta.2010.05.072.
13. Zinth, V., von Lüders, C., Hofmann, M., Hattendorff, J., Buchberger, I., Erhard, S., Rebelo-Kornmeier, J., Jossen, A., and Gilles, R. (2014). Lithium plating in lithium-ion batteries at sub-ambient temperatures investigated by in situ neutron diffraction. J. Power Sourc. *271*, 152–159. https://doi.org/10.1016/j.jpowsour.2014.07.168.
14. Diao, W., Saxena, S., and Pecht, M. (2019). Accelerated cycle life testing and capacity degradation modeling of LiCoO2-graphite cells. J. Power Sources *435*, 226830. https://doi.org/10.1016/j.jpowsour.2019.226830.
15. Waldmann, T., Wilka, M., Kasper, M., Fleischhammer, M., and Wohlfahrt-Mehrens, M. (2014). Temperature dependent ageing mechanisms in Lithium-ion batteries – A Post-Mortem study. J. Power Sourc. *262*, 129–135. https://doi.org/10.1016/j.jpowsour.2014.03.112.
16. Liu, L., Park, J., Lin, X., Sastry, A.M., and Lu, W. (2014). A thermal-electrochemical model that gives spatial-dependent growth of solid electrolyte interphase in a Li-ion battery. J. Power Sourc. *268*, 482–490. https://doi.org/10.1016/j.jpowsour.2014.06.050.
17. Sun, S., Guan, T., Shen, B., Leng, K., Gao, Y., Cheng, X., and Yin, G. (2017). Changes of Degradation Mechanisms of LiFePO4/Graphite Batteries Cycled at Different Ambient Temperatures. Electrochim. Acta *237*, 248–258. https://doi.org/10.1016/j.electacta.2017.03.158.
18. Xu, K. (2004). Nonaqueous Liquid Electrolytes for Lithium-Based Rechargeable Batteries. Chem. Rev. *104*, 4303–4417. https://doi.org/10.1021/cr030203g.
19. Somerville, L., Bareño, J., Trask, S., Jennings, P., McGordon, A., Lyness, C., and Bloom, I. (2016). The effect of charging rate on the graphite electrode of commercial lithium-ion cells: A post-mortem study. J. Power Sourc. *335*, 189–196. https://doi.org/10.1016/j.jpowsour.2016.10.002.
20. Guan, T., Sun, S., Yu, F., Gao, Y., Fan, P., Zuo, P., Du, C., and Yin, G. (2018). The degradation of LiCoO2/graphite batteries at different rates. Electrochim. Acta *279*, 204–212. https://doi.org/10.1016/j.electacta.2018.04.197.
21. Grützke, M., Kraft, V., Hoffmann, B., Klamor, S., Diekmann, J., Kwade, A., Winter, M., and Nowak, S. (2015). Aging investigations of a lithium-ion battery electrolyte from a field-tested hybrid electric vehicle. J. Power Sourc. *273*, 83–88. https://doi.org/10.1016/j.jpowsour.2014.09.064.
22. Yang, L., Takahashi, M., and Wang, B. (2006). A study on capacity fading of lithium-ion battery with manganese spinel positive electrode during cycling. Electrochim. Acta *51*, 3228–3234. https://doi.org/10.1016/j.electacta.2005.09.014.
23. Sun, S., Guan, T., Cheng, X., Zuo, P., Gao, Y., Du, C., and Yin, G. (2018). Accelerated aging and degradation mechanism of $LiFePO_4$/graphite batteries cycled at high discharge rates. RSC Adv. *8*, 25695–25703. https://doi.org/10.1039/C8RA04074E.
24. Pastor-Fernández, C., Dhammika Widanage, W., Marco, J., Gama-Valdez, M.-Á., and Chouchelamane, G.H. (2016). Identification and quantification of ageing mechanisms in Lithium-ion batteries using the EIS technique. In 2016 IEEE Transportation Electrification Conference and Expo (ITEC) (IEEE), pp. 1–6. https://doi.org/10.1109/ITEC.2016.7520198.
25. He, H., Liu, Y., Liu, Q., Li, Z., Xu, F., Dun, C., Ren, Y., Wang, M.x., and Xie, J. (2013). Failure Investigation of $LiFePO_4$ Cells in Over-Discharge Conditions. J. Electrochem. Soc. *160*, A793–A804. https://doi.org/10.1149/2.039306jes.
26. Yu, K., Wang, H., Mao, L., He, Q., and Wu, Q. (2022). IC Curve-Based Lithium-Ion Battery SOC Estimation at High Rate Charging Current. IEEE Trans. Instrum. Meas. *71*, 1–9. https://doi.org/10.1109/TIM.2022.3160554.
27. Meng, J., Du, X., Peng, J., Lin, M., and Song, Z. (2024). Rapid Lithium-Ion Battery Impedance Measurements Using Binary Sequence With Optimized Frequency Components. IEEE Trans. Ind. Electron. *71*, 7190–7198. https://doi.org/10.1109/TIE.2023.3306426.
28. Meng, J., Peng, J., Cai, L., and Song, Z. (2024). Rapid Impedance Extraction for Lithium-Ion Battery by Integrating Power Spectrum and Frequency Property. IEEE Trans. Ind. Electron. *71*, 7220–7229. https://doi.org/10.1109/TIE.2023.3301515.
29. Wikner, E., and Thiringer, T. (2018). Extending Battery Lifetime by Avoiding High SOC. Appl. Sci. *8*, 1825. https://doi.org/10.3390/app8101825.
30. Björklund, E., Wikner, E., Younesi, R., Brandell, D., and Edström, K. (2018). Influence of state-of-charge in commercial LiNi0.33Mn0.33Co0.33O2/LiMn2O4-graphite cells analyzed by synchrotron-based photoelectron spectroscopy. J. Energy Storage *15*, 172–180. https://doi.org/10.1016/j.est.2017.11.010.
31. Wikner, E., Björklund, E., Fridner, J., Brandell, D., and Thiringer, T. (2021). How the utilised SOC window in commercial Li-ion pouch cells influence battery ageing. J. Power Sourc. Adv. *8*, 100054. https://doi.org/10.1016/j.powera.2021.100054.
32. Ma, Z., Jiang, J., Wang, Z., Shi, W., Zheng, L., and Zhang, Y. (2014). A Research on SOC Estimation for LiFePO4 Battery with Graphite Negative Electrode Based on Incremental Capacity Analysis. Automot. Eng. *36*, 1439–1444. https://doi.org/10.19562/j.chinasae.qcgc.2014.12.004.
33. Guo, Q., Zhang, C., Gao, Y., Jiang, J., and Jiang, Y. (2018). Incremental Capacity Curve Based State of Health Estimation for LNMCO Lithium-ion Batteries. J. Glob. Ener. Interconn. *1*, 180–187. https://doi.org/10.19705/j.cnki.issn2096-5125.2018.02.011.
34. Dubarry, M., Truchot, C., Liaw, B.Y., Gering, K., Sazhin, S., Jamison, D., and Michelbacher, C. (2011). Evaluation of commercial lithium-ion cells based on composite positive electrode for plug-in hybrid electric vehicle applications. Part II. Degradation mechanism under 2C cycle aging. J. Power Sourc. *196*, 10336–10343. https://doi.org/10.1016/j.jpowsour.2011.08.078.
35. Dubarry, M., Truchot, C., Cugnet, M., Liaw, B.Y., Gering, K., Sazhin, S., Jamison, D., and Michelbacher, C. (2011). Evaluation of commercial lithium-ion cells based on composite positive electrode for plug-in hybrid electric vehicle applications. Part I: Initial characterizations. J. Power Sourc. *196*, 10328–10335. https://doi.org/10.1016/j.jpowsour.2011.08.077.
36. Liu, Y., Wang, L., Li, D., and Wang, K. (2023). State-of-health estimation of lithium-ion batteries based on electrochemical impedance spectroscopy: a review. Protect. Control Modern Power Syst. *8*, 41. https://doi.org/10.1186/s41601-023-00314-w.
37. Ning, G., Haran, B., and Popov, B.N. (2003). Capacity fade study of lithium-ion batteries cycled at high discharge rates. J. Power Sources *117*, 160–169. https://doi.org/10.1016/S0378-7753(03)00029-6.
38. An, S.J., Park, J.Y., Song, J., Lee, J., Kim, G.H., Yoon, J., and Oh, B. (2020). A fast method for evaluating stability of lithium ion batteries at high C-rates. J. Power Sourc. *480*, 228856. https://doi.org/10.1016/j.jpowsour.2020.228856.
39. Gao, Y., Jiang, J., Zhang, C., Zhang, W., and Jiang, Y. (2018). Aging mechanisms under different state-of-charge ranges and the multi-indicators system of state-of-health for lithium-ion battery with Li(NiMnCo)O2 cathode. J. Power Sourc. *400*, 641–651. https://doi.org/10.1016/j.jpowsour.2018.07.018.
40. Burow, D., Sergeeva, K., Calles, S., Schorb, K., Börger, A., Roth, C., and Heitjans, P. (2016). Inhomogeneous degradation of graphite anodes in automotive lithium ion batteries under low-temperature pulse cycling conditions. J. Power Sourc. *307*, 806–814. https://doi.org/10.1016/j.jpowsour.2016.01.033.
41. Gonzalez Malabet, H.J., Cavalheiro, G.M., Iriyama, T., Gabhart, A., Nelson, G.J., and Zhang, G. (2021). Electrochemical and Post-Mortem Degradation Analysis of Parallel-Connected Lithium-Ion Cells with Non-Uniform Temperature Distribution. J. Electrochem. Soc. *168*, 100507. https://doi.org/10.1149/1945-7111/ac2a7c.
42. Gao, Y., Jiang, J., Zhang, C., Zhang, W., Ma, Z., and Jiang, Y. (2017). Lithium-ion battery aging mechanisms and life model under different charging stresses. J. Power Sourc. *356*, 103–114. https://doi.org/10.1016/j.jpowsour.2017.04.084.
43. Ma, Z., Jiang, J., Shi, W., Zhang, W., and Mi, C.C. (2015). Investigation of path dependence in commercial lithium-ion cells for pure electric bus applications: Aging mechanism identification. J. Power Sourc. *274*, 29–40. https://doi.org/10.1016/j.jpowsour.2014.10.006.
44. Gering, K.L., Sazhin, S.V., Jamison, D.K., Michelbacher, C.J., Liaw, B.Y., Dubarry, M., and Cugnet, M. (2011). Investigation of path dependence in commercial lithium-ion cells chosen for plug-in hybrid vehicle duty cycle protocols. J. Power Sourc. *196*, 3395–3403. https://doi.org/10.1016/j.jpowsour.2010.05.058.
45. Yoshida, T., Takahashi, M., Morikawa, S., Ihara, C., Katsukawa, H., Shiratsuchi, T., and Yamaki, J.i. (2006). Degradation Mechanism and Life Prediction of Lithium-Ion Batteries.

J. Electrochem. Soc. *153*, A576. https://doi.org/10.1149/1.2162467.

46. Ando, K., Matsuda, T., and Imamura, D. (2018). Degradation diagnosis of lithium-ion batteries with a LiNi0.5Co0.2Mn0.3O2 and LiMn2O4 blended cathode using dV/dQ curve analysis. J. Power Sourc. *390*, 278–285. https://doi.org/10.1016/j.jpowsour.2018.04.043.

47. Zhe, Z.J.L.X.H.Y. (2016). Lithium Plating Identification from Degradation Behaviors of Lithium-Ion Cells. J. Electrochem. *22*, 607. https://doi.org/10.13208/j.electrochem.160561.

48. Chowdhury, N.R., Smith, A.J., Frenander, K., Mikheenkova, A., Lindström, R.W., and Thiringer, T. (2024). Influence of state of charge window on the degradation of Tesla lithium-ion battery cells. J. Energy Storage *76*, 110001. https://doi.org/10.1016/j.est.2023.110001.

STAR★METHODS

KEY RESOURCES TABLE

REAGENT or RESOURCE	SOURCE	IDENTIFIER
Other		
Negative electrode	Graphite	N/A
Electrolyte	LiPF6 in 1:2 EC: DMC	N/A
Positive electrode	$LiFePO_4$	N/A
NEWARE CT-4008-5V-12A	Charging and discharging	https://www.neware-technology.com
Software		
OriginLab	Analyze and graph	https://www.originlab.com

RESOURCE AVAILABILITY

Lead contact

Further information and requests for resources and reagents should be directed to and will be fulfilled by the lead contact, Yongsheng Wang (wysh@whut.edu.cn).

Materials availability

This study did not generate new unique reagents.

Data and code availability

- data reported in this paper will be shared by the lead contact upon request.
- This paper does not report original code.
- Any additional information required to reanalyze the data reported in this paper is available from the lead contact upon request.

METHOD DETAILS

The Zero-sum pulse proposed in the work is characterized by a high-rate symmetric charging and discharging current pulse. Parasitic reaction consumes a part of the applied current and makes capacity loss. This results in a lower amount of current being used for the practical charge. Therefore, the existence of parasitic reactions causes the capacity to be lower than it was before the Zero-sum pulse. Using this principle, the aging mechanisms at a specific SOC level can be explore, and this method can significantly degrade a battery at a specific SOC level in less than a week. By coordinating with the IC curve and EIS curve, the Zero-sum pulse method enables effective and timely analysis of aging mechanisms at various SOC levels.